EMBRY-RIDDLE
Aeronautical University™
SCHOLARLY COMMONS

Publications

12-13-2021

Reduced-order Dynamic Modeling and Robust Nonlinear Control of Fluid Flow Velocity Fields

Anu Kossery Jayaprakash
Embry-Riddle Aeronautical University, kosserya@my.erau.edu

William MacKunis
Embry-Riddle Aeronautical University, mackuniw@erau.edu

Vladimir Golubev
Embry-Riddle Aeronautical University, golubd1b@erau.edu

Oksana Stalnov
Technion-Israel Institute of Technology, oksana.s@techion.ac.il

Follow this and additional works at: https://commons.erau.edu/publication

Part of the Aerodynamics and Fluid Mechanics Commons, Dynamical Systems Commons, and the Fluid Dynamics Commons

Reduced-order Dynamic Modeling and Robust Nonlinear Control of Fluid Flow Velocity Fields

Anu Kossery Jayaprakash[1], William MacKunis[1], Vladimir Golubev[2] and Oksana Stalnov[3]

Abstract— A robust nonlinear control method is developed for fluid flow velocity tracking, which formally addresses the inherent challenges in practical implementation of closed-loop active flow control systems. A key challenge being addressed here is flow control design to compensate for model parameter variations that can arise from actuator perturbations. The control design is based on a detailed reduced-order model of the actuated flow dynamics, which is rigorously derived to incorporate the inherent time-varying uncertainty in the both the model parameters and the actuator dynamics. To the best of the authors' knowledge, this is the first robust nonlinear closed-loop active flow control result to prove exponential tracking control of a reduced-order actuated flow dynamic model, which formally incorporates input-multiplicative time-varying parametric uncertainty and nonlinear coupling between the state and control signal. A rigorous Lyapunov-based stability analysis is utilized to prove semi-global exponential tracking of a desired flow field velocity profile over a given spatial domain. A detailed comparative numerical study is provided, which demonstrates the performance improvement that is achieved using the proposed robust nonlinear flow control method to compensate for model uncertainty and uncertain actuator dynamics.

I. INTRODUCTION

Significant theoretical challenges exist in control design for fluid flow systems due to the fact that the governing dynamic equations are partial differential equations (PDEs) (e.g., Navier-Stokes equations), which are not amenable to control design. To address this challenge, model order reduction techniques are popularly utilized to develop control-oriented mathematical models for the flow dynamics. In practical applications, reduced-order models (ROM) can be developed using data obtained from experimental or high-fidelity computational methods. The resulting ROM are based on a given, fixed set of flow field conditions, so ROM dynamic uncertainty and unmodeled, time-varying parameter fluctuations are an inherent challenge in flow control applications. Moreover, in closed-loop active flow control systems, the controlling actuator itself can contribute significantly to ROM parameter fluctuations. For reliable flow control under realistic, time-varying operating conditions, rigorous control design methods are needed to address these inherent practical challenges.

Reliable control of fluid flow dynamic systems is critical in a wide range of engineering applications to achieve aerodynamic drag reduction [1], [2], aeroacoustic noise reduction [3], [4], and lift enhancement in aircraft [5], [6]. In order to achieve reliable performance over a wide range of operating conditions, closed-loop AFC offers many potential benefits over PFC and open loop AFC methods.

Experimental investigations of AFC systems have been widely presented in recent research [7]–[12]. Applications addressed in these experimental AFC studies include thermal protection [7]; control of vortex-body interaction and wing-tip-vortex meandering in NACA0012 airfoils [8], [9]; low-pressure gas turbines [10]; pressure, force, and moment manipulation in airfoils without moving control surfaces [11]; and flow separation control for performance enhancement in aircraft rudders [12]. Although all of the aforementioned studies have shown promising results in their respective objectives, most of them do not utilize rigorous mathematical tools to model the flow field dynamics and theoretically predict and analyze the influence of AFC on the flow. Dynamic modeling and mathematical analytical techniques can be leveraged to reduce the number of required repetitions and, hence, the time and cost that can be involved in numerical and experimental methods. A key element in the design and analysis of closed-loop AFC systems is the development of control-oriented ROMs.

Proper orthogonal decomposition (POD) [13], which is often referred to as Karhunen-Loève expansion or principal component analysis, is a method that can be used to obtain lower-dimensional dynamic models for fluid flow. POD is utilized to develop a set of basis functions (POD modes) that approximates the governing infinite-dimensional flow dynamics (i.e., the Navier-Stokes PDE) as a finite-dimensional set of ordinary differential equations (ODE) in terms of the POD modes. Depending on the flow control application and objectives, the number of POD modes in the ROM can be judiciously selected to yield the desired trade-off between ROM accuracy and computational efficiency. In application, the POD-based reduced-order flow dynamic model represents a nominal approximation of flow dynamics that is obtained under a specific set of flow field conditions (e.g., from experimental or high-fidelity computational data). In order to develop reliable closed-loop AFC over realistic, uncertain, time-varying flow field conditions, the control design must formally incorporate the uncertainty inherent in the reduced-order dynamic model.

[1]Anu Kossery Jayaprakash and William MacKunis are with the Physical Sciences Department, Embry Riddle Aeronautical University, Daytona Beach, FL 32114 `kosserya@my.erau.edu`, `mackuniw@erau.edu`

[2]Vladimir Golubev is with the Aerospace Engineering Department, Embry Riddle Aeronautical University, Daytona Beach, FL 32114., `golubd1b@erau.edu`

[3]Oksana Stalnov is with the Aerospace Engineering Department, Technion - Israel Institute of Technology, Haifa, Israel., `oksana.s@technion.ac.il`.

3978

To address the challenge of model uncertainty, various linear, robust, and intelligent methods for closed-loop AFC have been presented in recent research literature [14]–[20]. The techniques utilized in these recently developed flow control systems include, adaptive control [14], [15], PI control [16], and neural network-based control [17], [18]. While methods such as these have been widely shown to achieve promising results, robust nonlinear control approaches are less popularly utilized in flow control applications.

In this paper, a robust controller is presented, which is rigorously proven to achieve exponential tracking of a fluid flow velocity field. To the best of the authors' knowledge, this is the first robust nonlinear closed-loop AFC result to prove exponential tracking control of a POD-based reduced-order model for the complete actuated flow dynamics, which formally incorporates both input-multiplicative time-varying parametric uncertainty and nonlinear couplings between the state and control input. The three main contributions of this paper are as follows:

1) POD-based ROM development of the actuated flow dynamics, which formally incorporates the time-varying parameter fluctuations caused by unmodeled effects and control input perturbations.

2) A rigorous Lyapunov-based stability analysis which proves semi-global exponential tracking of a desired flow field velocity in the presence of input-multiplicative time-varying parametric uncertainty and nonlinear coupling between the state and control input.

3) A detailed comparative numerical study, which shows the performance improvement that is achieved using the proposed robust nonlinear control design under input-multiplicative uncertainty.

II. Dynamic Model and Properties

In this section, a POD-based model reduction technique is utilized to derive a reduced-order, control-oriented model for the actuated flow dynamics. The design of a robust nonlinear control law that formally incorporates the complete nonlinear dynamics and time-varying parametric uncertainty of the ROM is one of the key contributions of the current work.

A. Reduced order Model for Flow Field Dynamics

The incompressible Navier-Stokes equations are given as [21]

$$\nabla \cdot u = 0, \qquad \frac{\partial u}{\partial t} = -(u \cdot \nabla)u + \frac{1}{Re}\nabla^2(u) - \nabla p \quad (1)$$

where $u(s,t) : \Gamma \times [0,\infty) \in \mathbb{R}^3$ denotes the velocity of the flow field over a spatial domain $s \in \Gamma \subset \mathbb{R}^3$; $p(s,t) \in \mathbb{R}^3$ is the space- and time-dependent pressure of the flow field over Γ; and Re denotes the Reynolds number.

POD expansion or principal component analysis is used to obtain lower-dimensional dynamic models for fluid flow. In the POD modal decomposition technique, the flow velocity field $u(s,t)$ is expanded as a weighted sum of actuated and unactuated POD modes defined in the spatial domain Γ. The actuation effects are embedded in the coefficients of the Galerkin system. Specifically, the actuation effects can be included in the reduced-order model by defining the modal decomposition as [20]

$$u(s,t) = u_0 + \sum_{i=1}^{n} x_i(t)\phi_i(s) + \sum_{i=1}^{m} \gamma_i(t)\psi_i(s) \qquad (2)$$

In (2), $\phi_i(s) \in \mathbb{R}^3$, $i = 1,...,n$, denote the unactuated POD modes and $x_i(t)$, $i = 1,...,n$, denote time-varying coefficients resulting from the modal decomposition; and $u_0 \in \mathbb{R}^3$ denotes the mean flow velocity over Γ; $\psi_i(s) \in \mathbb{R}$ denote the actuation modes, and $\gamma_i(t) \in \mathbb{R}$ denote actuation values (i.e., control inputs). By leveraging an input separation method similar to that in [22], the actuation modes can be defined as the modes that minimize the energy not captured in the modal expansion of the actuated flow field.

By substituting the decomposition in (2) into (1), the complete actuated POD-based reduced-order model is obtained as

$$\begin{aligned}
\dot{x}_k = {} & A_k + \sum_{i=1}^{n} B_{ki}x_i(t) + \sum_{i=1}^{n}\sum_{j=1}^{n} C_{kij}x_i(t)x_j(t) \\
& + \sum_{i=1}^{m} D_{ki}\dot{\gamma}_i(t) + \sum_{i=1}^{n}\sum_{j=1}^{m} E_{kij}x_i(t)\gamma_j(t) \\
& + \sum_{i=1}^{m} F_{ki}\gamma_i(t) + \sum_{i=1}^{m}\sum_{j=1}^{m} G_{kij}\gamma_i(t)\gamma_j(t) \qquad (3)
\end{aligned}$$

In (3), A_k, B_{ki}, $C_{kij} \in \mathbb{R}$, for $k,i,j = 1,...,n$; D_{ki}, F_{ki}, $G_{kij}, k,i,j = 1,...,m$; and $E_{kij} \in \mathbb{R}$, for $k,i = 1,...,n$, and for $j = 1,... \ m$, represent constant uncertain parameters, which can be explicitly computed for any given, fixed set of numerical or experimental flow field data. Also in (3), $\dot{\gamma}_i(t)$, $i = 1,...,n$, represent the elements of the control input vector, which can be physically interpreted as a controllable perturbation to the flow field.

Property 1. *Since the fluid flow velocity $u(s,t)$ is based only on physical data collected from high-fidelity computational fluid dynamics (CFD) simulations or experiment, the decomposition in (2) can be used to prove that the actuation signal $\gamma(t)$ is bounded provided $x(t)$ is bounded.*

Remark 1. *(**Inherent Parameter Variations**) The POD-based reduced-order flow dynamic model in (3) is obtained from data collected under a single, fixed set of flow field conditions in the absence of actuation. The introduction of an actuation signal into the flow dynamic system causes fluctuations in the parameters (i.e., $A,...,G$) of the reduced-order model. Thus, to achieve reliable control of a flow field under realistic uncertain conditions, compensation for time-varying parametric uncertainty in the reduced-order model is of crucial importance for closed-loop flow control applications.*

B. Control-oriented Flow Dynamic Model

To address the time-varying parametric uncertainty inherent in the reduced-order model for the fluid flow dynam-

ics in (3), the dynamic model will be rewritten in control-oriented form as

$$
\begin{aligned}
\dot{x} &= f_1(x, x, \theta_1(t)) + f_2(x, \gamma, \theta_2(t)) \\
&\quad + f_3(\gamma, \gamma, \theta_3(t)) + \Omega(t)v
\end{aligned}
\tag{4}
$$

where $f_1(\cdot)$, $f_2(\cdot)$, $f_3(\cdot) \in \mathbb{R}^n$ denote uncertain nonlinear (quadratic) terms for which the kth rows are explicitly defined as

$$
f_{1,k}(x, \theta_1(t)) \triangleq A_k + \sum_{i=1}^{n} B_{ki} x_i(t) + \sum_{i=1}^{n} \sum_{j=1}^{n} C_{kij} x_i(t) x_j(t)
\tag{5}
$$

$$
f_{2,k}(x, \gamma, \theta_2(t)) \triangleq \sum_{i=1}^{n} \sum_{j=1}^{m} E_{kij} x_i(t) \gamma_j(t)
\tag{6}
$$

$$
f_{3,k}(\gamma, \theta_3(t)) \triangleq \sum_{i=1}^{m} F_{ki} \gamma_i(t) + \sum_{i=1}^{m} \sum_{j=1}^{m} G_{kij} \gamma_i(t) \gamma_j(t)
\tag{7}
$$

for $k = 1, \dots, n$. In (4) and (5), $x(t) \triangleq [\ x_1(t)\ \cdots\ x_n(t)\ ]^T \in \mathbb{R}^n$ denotes the state vector, $v(t) \triangleq \dot{\gamma}(t) \in \mathbb{R}^m$ is the control input; and $\theta_1(t) \in \mathbb{R}^{n^2+n+1}$, $\theta_2(t) \in \mathbb{R}^{n^2}$, $\theta_3(t) \in \mathbb{R}^{n^2+n}$, for $k = 1, \dots, n$, denote vectors containing the uncertain time-varying parameters in the dynamic model. Also in (4), $\Omega(t) \in \mathbb{R}^{n \times m}$ denotes an uncertain input gain matrix. Specifically, $\Omega(t)$ contains the terms D_{ki}, for $k = 1, \dots, n$, $i = 1, \dots, m$, which are introduced in (3).

Remark 2. (Control Input Variable) *The control input term $v(t)$ is being defined for notational convenience only. The subsequent control development and stability analysis will incorporate the input-dependent actuation signals $\gamma(t)$ to formally address the challenge of input-multiplicative uncertainty.*

Assumption 1. *The reduced-order model in (4) is assumed to be controllable.*

Assumption 2. *The parameter vectors $\theta_1(t)$, $\theta_2(t)$, $\theta_3(t)$ and the parameter matrix $\Omega(t)$ and their derivatives satisfy the following inequalities:*

$$
\begin{aligned}
\|\theta_1(t)\| &\leq \zeta_1 \quad \|\theta_2(t)\| \leq \zeta_2 \quad \|\theta_3(t)\| \leq \zeta_3 \\
\|\dot{\theta}_1(t)\| &\leq \zeta_{1d} \quad \|\dot{\theta}_2(t)\| \leq \zeta_{2d} \quad \|\dot{\theta}_3(t)\| \leq \zeta_{3d} \\
\sup_t\{\|\Omega(t)\|_{i\infty}\} &\leq \zeta_\Omega \quad \sup_t\{\|\dot{\Omega}(t)\|_{i\infty}\} \leq \zeta_{\Omega d}
\end{aligned}
\tag{8}
$$

where ζ_1, ζ_2, ζ_3, ζ_Ω, ζ_{1d}, ζ_{2d}, ζ_{3d}, $\zeta_{\Omega d} \in \mathbb{R}^+$ are known bounding constants. As is standard in robust nonlinear control methods, knowledge of the upper bounds on the uncertain parameters is utilized to derive sufficient gain conditions in the subsequent stability analysis.

Assumption 3. (Fully Actuated System) *The subsequent analysis is based on the assumption that the the number m of actuation modes is equal to the number n of unactuated modes (i.e., it is assumed that $n = m$ in (4)). However, the adaptive control design presented here can be applied to any system for which $m \geq n$.*

III. Control Development

A. Control Objective

The control objective is to ensure that the state $x(t)$ tracks a desired flow field velocity profile $x_d(t) \in \mathbb{R}^n$. To quantify this control objective, a tracking error variable $e(t) \in \mathbb{R}^n$ is defined as

$$
e \triangleq x - x_d.
\tag{9}
$$

To facilitate the subsequent analysis, an auxiliary (filtered) tracking error variable, denoted by $r(t) \in \mathbb{R}^n$, is defined as

$$
r \triangleq \dot{e} + \alpha e
\tag{10}
$$

where $\alpha \in \mathbb{R}^{n \times n}$ is a positive definite, constant control gain matrix.

Assumption 4. *The desired flow field velocity profile $x_d(t)$ is bounded and smooth in the sense that*

$$
x_d(t) \leq \zeta_{xd1}, \qquad \dot{x}_d(t) \leq \zeta_{xd2}, \qquad \ddot{x}_d(t) \leq \zeta_{xd3}
\tag{11}
$$

where ζ_{xd1}, ζ_{xd2}, $\zeta_{xd3} \in \mathbb{R}^+$ are known bounding constants.

B. Open-Loop Error System

The open-loop tracking error dynamics can be developed by taking the time derivative of (10) and using (4)–(9) to obtain

$$
\dot{r} = \ddot{x} - \ddot{x}_d = \dot{f}_1 + \dot{f}_2 + \dot{f}_3 + \dot{\Omega}v + \Omega\dot{v} - \ddot{x}_d + \alpha(r - \alpha e)
\tag{12}
$$

The open-loop error dynamics in (12) can be rewritten in compact form as

$$
\dot{r} = \tilde{N} + \tilde{N}_\gamma + N_d + \dot{\Omega}v + \Omega\dot{v} - e
\tag{13}
$$

where the uncertain nonlinear auxiliary terms $\tilde{N}(x, \dot{x}, x_d, \dot{x}_d, e, r, t) \in \mathbb{R}^n$, $\tilde{N}_\gamma(x, \dot{x}, \gamma) \in \mathbb{R}^n$, and $N_d(x_d, \dot{x}_d, \ddot{x}_d)$ are explicitly defined as

$$
\tilde{N}_\gamma \triangleq \gamma^T E_k^T \dot{x} + x^T \dot{E}_k \gamma + \dot{F}_k \gamma + \gamma^T \dot{G}_k \gamma
\tag{14}
$$

$$
\begin{aligned}
\tilde{N} \triangleq\ & \dot{B}_k(x - x_d) + B_k(\dot{x} - \dot{x}_d) \\
& + x^T(C_k + C_k^T)\dot{x}_d - x_d^T(C_k + C_k^T)\dot{x}_d \\
& + x^T(C_k + C_k^T)\dot{x} - x^T(C_k + C_k^T)\dot{x}_d \\
& + x^T \dot{C}_k x - x_d^T \dot{C}_k x_d + \alpha(r - \alpha e) + e
\end{aligned}
\tag{15}
$$

$$
\begin{aligned}
N_d =\ & \dot{B}_k x_d + B_k \dot{x}_d + x_d^T(C_k + C_k^T)\dot{x}_d \\
& + x_d^T \dot{C}_k x_d - \ddot{x}_d
\end{aligned}
\tag{16}
$$

Motivation for the selective grouping of terms in (14)–(16) is based on the fact that the following bounding inequalities can be developed[1]

$$
\|\tilde{N}\| \leq \rho_1(\|z\|)\|z\|, \quad \|N_d\| \leq \zeta_{Nd}
\tag{17}
$$

$$
\|\tilde{N}_\gamma\| \leq \Xi_1\|\gamma\|^2 + \Xi_2\|\gamma\| + \rho_\gamma(\|z\|)\|z\|
\tag{18}
$$

where ζ_{Nd}, Ξ_1, $\Xi_2 \in \mathbb{R}^+$ are known bounding constants; $\rho_1(\cdot)$ and $\rho_\gamma(\cdot)$ are positive, globally invertible non-decreasing functions; and $z(t) \in \mathbb{R}^{2n}$ is defined as

$$
z \triangleq [\ e^T \quad r^T\ ]^T.
\tag{19}
$$

---

[1]Proof of the bound on the auxiliary terms is straightforward using the mean-value theorem and Young's Inequality and is omitted here for brevity.

Note that the bounding of $N_d(x_d, \dot{x}_d, \ddot{x}_d)$ follows directly from Assumption 4 and Inequalities (11).

C. Control Design and Closed-loop Error System

Based on the open loop error dynamics in (13) and the subsequent stability analysis, the control input is designed via

$$v = -\Omega_0^{-1}[(k_s + I_n)e(t) - (k_s + I_n)e(0) + \omega] \qquad (20)$$

where $\omega(t) \in R^n$ is an implicit learning law with an update rule defined as

$$\begin{aligned} \dot{\omega} &= \alpha(k_s + I_n)e(t) + k_v\|v\|\,\mathrm{sgn}(r) \\ &\quad + (k_\beta + k_{\gamma 1}\|\gamma\| + k_{\gamma 2}\|\gamma\|^2)\,\mathrm{sgn}(r) \end{aligned} \qquad (21)$$

and k_s, k_v, k_β, $k_{\gamma 1}$, $k_{\gamma 2} \in \mathbb{R}^{n \times n}$ denote positive-definite, diagonal, control gain matrices. In (20), $\Omega_0 \in \mathbb{R}^n$ is a matrix containing the constant, known, nominal values of the uncertain parameters in Ω; $\mathrm{sgn}(\cdot)$ denotes the standard signum function, where the function is applied element-wise to the vector argument; and I_n denotes the $n \times n$ identity matrix.

After taking the time derivative of (20) and substituting the result into the open-loop error dynamics in (13), the closed-loop error system can be expressed as

$$\begin{aligned} \dot{r} &= \tilde{N} + \tilde{N}_\gamma + N_d + \dot{\Omega}v - \tilde{\Omega}(k_s + I_n)r - e \\ &\quad - \tilde{\Omega}k_{\gamma 1}\|\gamma\|\,\mathrm{sgn}(r) - \tilde{\Omega}k_{\gamma 2}\|\gamma\|^2\,\mathrm{sgn}(r) \\ &\quad - \tilde{\Omega}k_v\|v\|\,\mathrm{sgn}(r) - \tilde{\Omega}k_\beta\,\mathrm{sgn}(r) \end{aligned} \qquad (22)$$

where (10) was utilized. In (22), the uncertain parameter mismatch matrix $\tilde{\Omega}(t) \in \mathbb{R}^{n \times n}$ is defined as

$$\tilde{\Omega} \triangleq \Omega\Omega_0^{-1}. \qquad (23)$$

To facilitate the subsequent stability analysis, the mismatch matrix $\tilde{\Omega}(t)$ in (23) will be separated into diagonal ($\Lambda(t) \in \mathbb{R}^{n \times n}$) and off-diagonal ($\Delta(t) \in \mathbb{R}^{n \times n}$) components as

$$\tilde{\Omega} = \Lambda + \Delta. \qquad (24)$$

Assumption 5. *Approximate knowledge of the parameter matrix $\Omega(t)$ is available such that the mismatch matrix $\tilde{\Omega}(t)$ is diagonally dominant in the sense that*

$$\inf_t\{\lambda_{\min}(\Lambda)\} - \sup_t\{\|\Delta\|_{i\infty}\} > \varepsilon \qquad (25)$$

where $\varepsilon \in \mathbb{R}^+$ is a known bounding constant.

Assumption 5 is mild in the sense that, for a given set of flow field data (e.g., from high-fidelity CFD simulation or experiment), the nominal values of the reduced-order model parameters would be readily available.

IV. STABILITY ANALYSIS

Theorem 1. *The control law given in Equations (20) and (21) ensures semi-global exponential tracking in the sense that*

$$\|e(t)\| \le \|z(0)\| \exp(-\frac{\lambda_1}{2}t) \qquad \forall\, t \in [0, \infty)$$

where $\lambda_1 \in \mathbb{R}^+$, provided k_s is selected sufficiently large (see the subsequent proof), and where the control gain matrices k_v, k_β, $k_{\gamma 1}$, and $k_{\gamma 2}$ introduced in (20) are selected to satisfy the sufficient conditions

$$\begin{aligned} \lambda_{\min}(k_v) &> \frac{\zeta_{\Omega d}}{\varepsilon} & \lambda_{\min}(k_\beta) &> \frac{\zeta_{Nd}}{\varepsilon} \\ \lambda_{\min}(k_{\gamma 1}) &> \frac{\Xi_1}{\varepsilon} & \lambda_{\min}(k_{\gamma 2}) &> \frac{\Xi_2}{\varepsilon} \end{aligned} \qquad (26)$$

where $\zeta_{\Omega d}$, ζ_{Nd}, Ξ_1, and Ξ_2 are introduced in (17); ε is introduced in (25); and $\lambda_{\min}(\cdot)$ denotes the minimum eigenvalue of the argument.

Proof: Let $V(z) : \mathbb{R}^{2n} \to \mathbb{R}$ be a continuously differentiable, positive-definite function defined as

$$V(z) \triangleq \frac{1}{2}e^T e + \frac{1}{2}r^T r \qquad (27)$$

where $e(t)$ and $r(t)$ are defined in (9) and (10), respectively. After taking the time derivative of (27) and using Equations (10), (22), and (25), along with Inequalities (8) and (25), $\dot{V}(z)$ can be upper bounded as

$$\begin{aligned} \dot{V}(z) &\le -\alpha\|e\|^2 + r^T(\tilde{N} + \tilde{N}_\gamma) - \varepsilon(\lambda_{\min}(k_s) + I_n)\|r\|^2 \\ &\quad + \zeta_{\Omega d}\|v\|\|r\| - \varepsilon\lambda_{\min}(k_v)\|v\|\|r\| + \zeta_{Nd}\|r\| - \varepsilon\lambda_{\min}(k_\beta)\|r\| \\ &\quad - \varepsilon\lambda_{\min}(k_{\gamma 1})\|\gamma\|\|r\| - \varepsilon\lambda_{\min}(k_{\gamma 2})\|\gamma\|^2\|r\| \end{aligned} \qquad (28)$$

where the fact that $|r| \ge \|r\| \,\forall\, r \in \mathbb{R}^n$ was used. After using the bounding inequalities in (17), combining terms, and rearranging, the upper bound in (28) can be expressed as

$$\begin{aligned} \dot{V}(z) &\le -\alpha\|e\|^2 - \varepsilon\|r\|^2 \\ &\quad - [\varepsilon\lambda_{\min}(k_s)\|r\|^2 - \rho(\|z\|)\|r\|\|z\|] \end{aligned} \qquad (29)$$

provided the gain conditions in (26) are satisfied, where $\rho(\|z\|) \triangleq \rho_1(\|z\|) + \rho_\gamma(\|z\|)$ is a positive. globally invertible non-decreasing function. By completing the squares for the bracketed terms, the upper bound in (29) can be expressed as

$$\dot{V}(z) \le -(\eta - \frac{\rho^2(\|z\|)}{4\varepsilon\lambda_{\min}(k_s)})\|z\|^2 \qquad (30)$$

where $z(t)$ is defined in (19), and $\eta \triangleq \min\{\alpha, \varepsilon\}$. The upper bound in (30) can be expressed as

$$\dot{V}(z) \le -\lambda_1\|z\|^2 \qquad (31)$$

where $\lambda_1 \in \mathbb{R}^+$ is a constant, provided $z(t)$ is within the domain defined by

$$\mathcal{S} \triangleq \{z \in \mathbb{R}^{2n} | \|z\| < \rho^{-1}(2\sqrt{\eta\varepsilon\lambda_{\min}(k_s)})\}.$$

The inequalities in (27) and (31) can be used to show that $V(z) \in \mathcal{L}_\infty$ in $\mathcal{S}$; hence, $e(t)$, $r(t) \in \mathcal{L}_\infty$ in $\mathcal{S}$. Given that $e(t)$, $r(t) \in \mathcal{L}_\infty$ in $\mathcal{S}$, Equation (10) can be used to show that $\dot{e}(t) \in \mathcal{L}_\infty$ in $\mathcal{S}$; and Assumption 4 can be used with Equations (9) and (10) to prove that $x(t)$, $\dot{x}(t) \in \mathcal{L}_\infty$ in $\mathcal{S}$. Given that $x(t) \in \mathcal{L}_\infty$ in $\mathcal{S}$, Property 1 can be used along with Equation (2) to show that $\gamma(t) \in \mathcal{L}_\infty$ in $\mathcal{S}$. Since $x(t)$, $\dot{x}(t)$, $\gamma(t) \in \mathcal{L}_\infty$ in $\mathcal{S}$, Assumption 2 can be used along with Equation (3) to prove that $\dot{\gamma}(t)$, $v(t) \in \mathcal{L}_\infty$

3981

in $\mathcal{S}$. Given that $r(t)$, $\gamma(t)$, $v(t) \in \mathcal{L}_\infty$ in $\mathcal{S}$, the time derivative of Equation (20) can be used with (21) to prove that $\dot{v}(t) \in \mathcal{L}_\infty$ in $\mathcal{S}$.

The definition of $V(z)$ in Equation (27) can be used along with Inequality (31) to show that $V(z)$ can be upper bounded as

$$\dot{V}(z) \le -\lambda_1 V(z) \tag{32}$$

in the domain $\mathcal{S}$. The differential inequality in (32) can be solved as

$$V(z) \le V(z(0)) \exp(-\lambda_1 t) \tag{33}$$

Hence, Equations (19), (27), and (33) can be used to conclude that

$$\|e(t)\| \le \|z(0)\| \exp\left(-\frac{\lambda_1}{2} t\right) \qquad \forall\, t \in [0, \infty) \tag{34}$$

V. SIMULATION

A detailed numerical simulation was created using Matlab/Simulink to demonstrate the performance of the proposed robust control law. The simulation demonstrates the performance of the control law in (20) and (21) for two cases: 1) with actuator uncertainty compensation and 2) without compensation. The control law with uncertainty compensation includes nonzero values of all of the control gains introduced in (20) and (21); and as a comparison, the control gains k_v, $k_{\gamma 1}$, and $k_{\gamma 2}$ in (21) are set to zero to simulate the control law without input-uncertainty compensation. The reduced-order flow dynamic model in the simulation uses four POD modes, but the proposed control design can be applied to ROM consisting of an arbitrary number of modes. The objective of the controller is to regulate the flow field velocity to a constant value. The regulation control objective is presented as a proof-of-concept only. The proposed control method could be applied to a tracking control objective with little modification. The flow field dynamic reduced-order model used in this simulation is given by [23]:

$$\dot{x}_1 = b_1(t) + L_{11}(t)x_1 + Q_{141}(t)x_1 x_4 + Q_{111}(t)x_1^2$$
$$+ Q_{121}(t)x_1 x_2 + Q_{131}(t)x_1 x_3 + \beta_1(t)\dot{\gamma}_1 \tag{35}$$

$$\dot{x}_2 = b_2(t) + [L_{22}(t) + R_2(t)(x_2^2 + x_3^2)]x_2$$
$$+ L_{23}(t)x_3 + Q_{212}(t)x_1 x_2 + \beta_2(t)\dot{\gamma}_2 \tag{36}$$

$$\dot{x}_3 = b_3(t) + L_{32}(t)x_2$$
$$+ [L_{33}(t) + R_3(x_2(t)^2 + x_3^2)]x_3$$
$$+ Q_{313}(t)x_1 x_3 + Q_{314}(t)x_1 x_4 + \beta_3(t)\dot{\gamma}_3 \tag{37}$$

$$\dot{x}_4 = b_4(t) + L_{41}(t)x_1 + L_{44}(t)x_4 + Q_{444}(t)x_4^2$$
$$+ Q_{414}(t)x_1 x_4(t) + Q_{424}(t)x_2 x_4$$
$$+ Q_{434}(t)x_3 x_4 + \beta_4(t)\dot{\gamma}_4 \tag{38}$$

To simulate a realistic closed-loop AFC scenario where the model parameters are influenced by the control perturbations, the parameters in the plant model in (35)–(38) are time-varying. For completeness in defining the simulation plant model, the nominal values of the time varying parameters $b_i(t), L_{ij}(t), Q_{ijk}(t)$ for $i; j; k = 1, ..., 4$ are provided in Table I and were taken from [23]. The initial conditions

of the states are $x_{10} = 2, x_{20} = 3, x_{30} = 6, x_{40} = 2$.

TABLE I

NOMINAL PARAMETERS USED IN THE SIMULATION PLANT MODEL

Linear Terms		Quadratic and Cubic Terms	
$b_{10} = 557.7$	$L_{11} = -86.1$	$Q_{111} = 1.8$	$Q_{414} = 2.9$
$b_{20} = 1016.9$	$L_{22} = -392.4$	$Q_{121} = -2.2$	$Q_{424} = -9.8$
$b_{30} = 41.0$	$L_{23} = 263.9$	$Q_{131} = -2.3$	$Q_{434} = 6.3$
$b_{40} = -628.9$	$L_{32} = -218.3$	$Q_{141} = -6.8$	$Q_{444} = -7.3$
	$L_{33} = -7.6$	$Q_{212} = 75.0$	
	$L_{41} = 43.4$	$Q_{313} = 5.0$	$R_2 = -2.5$
	$L_{44} = -113.5$	$Q_{314} = 3.9$	$R_3 = -0.2$

A. Summary of Results

The control gains in the simulation were selected as $k_v = 3.75 \times I_n, k_{\gamma_1} = 0.01 \times I_n, k_\beta = 2000 \times I_n$ (see Equations (20) and (21)). As stated previously, $k_v = k_{\gamma_1} = k_{\gamma_2} = 0$ for the control law without input uncertainty compensation. The control gains in the simulation were selected to yield the best performance tradeoff between regulation accuracy and control usage. In an attempt to reduce chattering, the discontinuous signum function was approximated in the simulation using a continuous logarithmic switching function without loss of generality. To provide a realistic demonstration of the closed-loop system performance under parametric uncertainty, the control system was simulated for 50 iterations of randomized time-varying parametric uncertainty in the plant model (i.e., using the Matlab rand function). Each iteration was tested over six different levels of randomized uncertainty: 5%, 7%, 10%, 15%, 18%, 20% (e.g., x% uncertainty in b_1 is mathematically defined via $b_1 = b_{10} \pm [(x\% \text{ of } b_{10}) \times \sin(t)]$, where b_{10} is the corresponding nominal parameter value in Table 1).
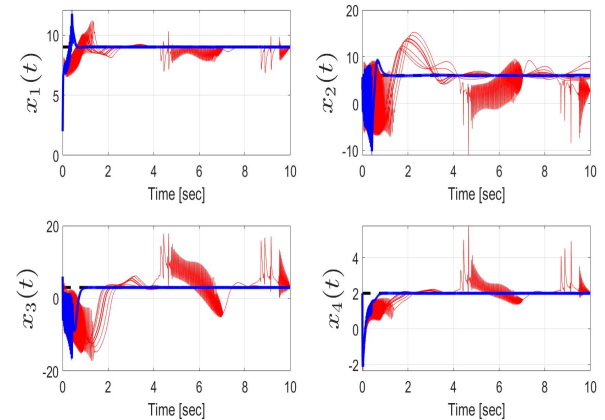

Fig. 1. Time evolution of the state $x_1(t), x_2(t), x_3(t), x_4(t)$ for controller without uncertainty compensation (**red**) and controller with uncertainty compensation (**blue**) during closed-loop operation for 50 iterations of randomized uncertainty.

Figure 1 shows the time evolution of the states during closed-loop operation for 50 iterations of 20% randomized uncertainty for the two cases: 1) with input uncertainty

compensation (in blue) and 2) without compensation (in red). Figure 2 shows the time evolution of the control input during the closed-loop operation for a given iteration of 20% uncertainty (for clarity of the figure, only one iteration is shown). These results clearly demonstrate the improved performance that can be achieved using the proposed controller with input uncertainty compensation.

The average mean squared error (MSE) in trajectory tracking over the 50 iterations was then calculated for each of the six levels of uncertainty for the two cases: 1) controller with compensation and 2) controller without compensation. In summary, the average MSE reduction achieved using the proposed compensator ranged from 37.39% to 72.10%.
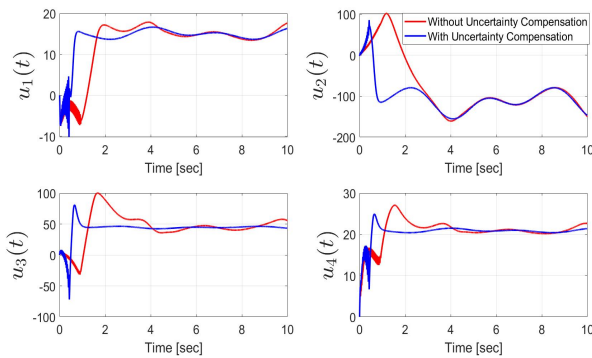

Fig. 2. Control input $u_1(t), u_2(t), u_3(t), u_4(t)$ during closed-loop trajectory tracking control operation without and with uncertainty compensation

VI. Conclusions

In this paper, a robust nonlinear flow control system is presented, which is shown to exponentially track a desired flow field velocity over a given spatial domain in the presence of time varying input-multiplicative parametric uncertainty and nonlinear coupling between the state and the control input. To achieve the result, a detailed ROM is derived, and a rigorous error system development and Lyapunov-based stability analysis are provided. The Lyapunov-based stability analysis proves that the control design achieves semi-global exponential tracking of the desired velocity profile. Numerical simulation results are also provided, which show the performance improvement of the proposed control law over a standard sliding mode control method in compensating for time-varying input-multiplicative uncertainty. The numerical simulation results show a reduction in the average MSE ranging from 37.39% up to 72.10% over multiple trials.

ACKNOWLEDGMENT

References

[1] A. R. Paul, A. Jain, and F. Alam, "Drag reduction of a passenger car using flow control techniques," *International Journal of Automotive Technology*, vol. 20, no. 2, pp. 397–410, 2019.

[2] S. Chae, S. Lee, J. Kim, and J. H. Lee, "Adaptive-passive control of flow over a sphere for drag reduction," *Physics of Fluids*, vol. 31, no. 1, p. 015107, 2019.

[3] W. Zhu, Z. Xiao, and S. Fu, "Numerical modeling screen for flow and noise control around tandem cylinders," *AIAA Journal*, 2020.

[4] C. Prasad and P. Morris, "A study of noise reduction mechanisms of jets with fluid inserts," *Journal of Sound and Vibration*, p. 115331, 2020.

[5] M. DeSalvo, E. Whalen, and A. Glezer, "High-lift performance enhancement using active flow control," *AIAA Journal*, pp. 1–15, 2020.

[6] L.-H. Feng, Z.-Y. Li, and Y.-L. Chen, "Lift enhancement strategy and mechanism for a plunging airfoil based on vortex control," *Physics of Fluids*, vol. 32, no. 8, p. 087116, 2020.

[7] J. Huang and W.-X. Yao, "Active flow control by a novel combinational active thermal protection for hypersonic vehicles," *Acta Astronautica*, vol. 170, pp. 320–330, 2020.

[8] A. Weingaertner, P. Tewes, and J. C. Little, "Parallel vortex body interaction enabled by active flow control," *Experiments in Fluids*, vol. 61, no. 137, p. 137, 2020.

[9] M. Dghim, M. Ferchichi, and H. Fellouah, "On the effect of active flow control on the meandering of a wing-tip vortex," *Journal of Fluid Mechanics*, vol. 896, p. A30, 2020.

[10] J. Bons, S. Benton, C. Bernardini, and M. Bloxham, "Active flow control for low-pressure turbines," *AIAA Journal*, vol. 56, no. 7, pp. 2687–2698, 2018.

[11] D. Dolgopyat and A. Seifert, "Active flow control virtual maneuvering system applied to conventional airfoil," *AIAA Journal*, vol. 57, no. 1, pp. 72–89, 2019.

[12] E. A. Whalen, A. Shmilovich, M. Spoor, J. Tran, P. Vijgen, J. C. Lin, and M. Andino, "Flight test of an active flow control enhanced vertical tail," *AIAA Journal*, vol. 56, no. 9, pp. 3393–3398, 2018.

[13] J. Weiss, "A tutorial on the proper orthogonal decomposition," in *AIAA Aviation 2019 Forum*, p. 3333, 2019.

[14] B. Choi, Y. Hong, B. Lee, M. Kim, H. J. Kim, and C. Kim, "Adaptive flow separation control over an asymmetric airfoil," *International Journal of Aeronautical and Space Sciences*, vol. 19, no. 2, pp. 305–315, 2018.

[15] V. Motta and L. Malzacher, "Open-loop and closed-loop flow control based on van der pol modeling," *Acta Mechanica*, vol. 229, no. 1, pp. 389–401, 2018.

[16] D. Xingya and F. Jianchao, "Closed-loop flow control of an ultra-compact serpentine inlet based on nondimensional model," *Chinese Journal of Aeronautics*, 2020.

[17] S. Shimomura, S. Sekimoto, A. Oyama, K. Fujii, and H. Nishida, "Closed-loop flow separation control using the deep q network over airfoil," *AIAA Journal*, pp. 1–11, 2020.

[18] J. Rabault, M. Kuchta, A. Jensen, U. Réglade, and N. Cerardi, "Artificial neural networks trained through deep reinforcement learning discover control strategies for active flow control," *arXiv preprint arXiv:1808.07664*, 2018.

[19] K. B. Kidambi, N. Ramos-Pedroza, W. MacKunis, and S. V. Drakunov, "Robust nonlinear estimation and control of fluid flow velocity fields," in *2016 IEEE 55th Conference on Decision and Control (CDC)*, pp. 6727–6732, IEEE, 2016.

[20] K. B. Kidambi, N. Ramos-Pedroza, W. MacKunis, and S. V. Drakunov, "A closed-loop nonlinear control and sliding mode estimation strategy for fluid flow regulation," *International Journal of Robust and Nonlinear Control*, vol. 29, no. 3, pp. 779–792, 2019.

[21] C. K. Batchelor and G. Batchelor, *An introduction to fluid dynamics*. Cambridge university press, 2000.

[22] C. Kasnakoğlu, A. Serrani, and M. Ö. Efe, "Control input separation by actuation mode expansion for flow control problems," *International Journal of Control*, vol. 81, no. 9, pp. 1475–1492, 2008.

[23] S. V. Gordeyev and F. O. Thomas, "A temporal proper decomposition (tpod) for closed-loop flow control," *Experiments in fluids*, vol. 54, no. 3, pp. 1–16, 2013.